

$^{179}\text{Ta}(n, \gamma)$ cross-section measurement and the astrophysical origin of the ^{180}Ta isotope

Garg, Ruchi; Dellmann, Sophia Florence; Lederer-Woods, C.; Bruno, C. G.; Eberhardt, K.; Geppert, C.; Heftrich, Tanja; Kajan, I.; Käppeler, F.; Phoenix, B.; Reifarth, Rene; Schumann, D.; Weigand, M.; Wheldon, Carl

DOI:

[10.1103/physrevc.107.045805](https://doi.org/10.1103/physrevc.107.045805)

License:

Creative Commons: Attribution (CC BY)

Document Version

Publisher's PDF, also known as Version of record

Citation for published version (Harvard):

Garg, R, Dellmann, SF, Lederer-Woods, C, Bruno, CG, Eberhardt, K, Geppert, C, Heftrich, T, Kajan, I, Käppeler, F, Phoenix, B, Reifarth, R, Schumann, D, Weigand, M & Wheldon, C 2023, '179Ta(n, γ) cross-section measurement and the astrophysical origin of the 180Ta isotope', *Physical Review C*, vol. 107, no. 4, 045805. <https://doi.org/10.1103/physrevc.107.045805>

[Link to publication on Research at Birmingham portal](#)

General rights

Unless a licence is specified above, all rights (including copyright and moral rights) in this document are retained by the authors and/or the copyright holders. The express permission of the copyright holder must be obtained for any use of this material other than for purposes permitted by law.

- Users may freely distribute the URL that is used to identify this publication.
- Users may download and/or print one copy of the publication from the University of Birmingham research portal for the purpose of private study or non-commercial research.
- User may use extracts from the document in line with the concept of 'fair dealing' under the Copyright, Designs and Patents Act 1988 (?)
- Users may not further distribute the material nor use it for the purposes of commercial gain.






Where a licence is displayed above, please note the terms and conditions of the licence govern your use of this document.

When citing, please reference the published version.

Take down policy

While the University of Birmingham exercises care and attention in making items available there are rare occasions when an item has been uploaded in error or has been deemed to be commercially or otherwise sensitive.

If you believe that this is the case for this document, please contact UBIRA@lists.bham.ac.uk providing details and we will remove access to the work immediately and investigate.

$^{179}\text{Ta}(n, \gamma)$ cross-section measurement and the astrophysical origin of the ^{180}Ta isotopeR. Garg ^{1,2,*}, S. Dellmann ³, C. Lederer-Woods,¹ C. G. Bruno,¹ K. Eberhardt,⁴ C. Geppert,⁴ T. Heftrich ³, I. Kajan,⁵
F. Käppeler,^{6,†} B. Phoenix,⁷ R. Reifarth ³, D. Schumann,⁵ M. Weigand,³ and C. Wheldon ⁷¹*School of Physics and Astronomy, University of Edinburgh, Edinburgh EH9 3FD, United Kingdom*²*Facility for Rare Isotope Beams, Michigan State University, East Lansing, Michigan 48824, USA*³*Goethe Universität Frankfurt, Frankfurt 60438, Germany*⁴*Johannes Gutenberg Universität Mainz, Mainz 55128, Germany*⁵*Paul Scherrer Institute, Villigen, Villigen 5232, Switzerland*⁶*Karlsruhe Institute of Technology, Campus North, Karlsruhe 76021, Germany*⁷*School of Physics and Astronomy, University of Birmingham, Birmingham B15 2TT, United Kingdom*

(Received 19 December 2022; accepted 6 March 2023; published 13 April 2023)

$^{180\text{m}}\text{Ta}$ is nature's rarest (quasi) stable isotope and its astrophysical origin is an open question. A possible production site of this isotope is the slow neutron capture process in asymptotic giant branch stars, where it can be produced via neutron capture reactions on unstable ^{179}Ta . We report a new measurement of the $^{179}\text{Ta}(n, \gamma)^{180}\text{Ta}$ cross section at thermal-neutron energies via the activation technique. Our results for the thermal and resonance-integral cross sections are 952 ± 57 and 2013 ± 148 b, respectively. The thermal cross section is in good agreement with the only previous measurement [Phys. Rev. C **60**, 025802 (1999)], while the resonance integral is different by a factor of ≈ 1.7 . While neutron energies in this work are smaller than the energies in a stellar environment, our results may lead to improvements in theoretical predictions of the stellar cross section.

DOI: [10.1103/PhysRevC.107.045805](https://doi.org/10.1103/PhysRevC.107.045805)**I. INTRODUCTION**

Tantalum-180 is one of the most interesting isotopes in nature. In its ground state, this isotope is unstable with a half-life of 8.15 hours, however, it has a high-spin (9^-) metastable state at 77.2 keV that has a half-life $> 7 \times 10^{15}$ years. This isomer, $^{180\text{m}}\text{Ta}$, is nature's rarest (quasi) stable isotope and its stellar origin remains an open question. At least three nucleosynthesis processes are thought to contribute to the ^{180}Ta abundance. References [1–4] suggest that ^{180}Ta is produced by $^{180}\text{Hf}(\nu_e, e)^{180}\text{Ta}$ and $^{181}\text{Ta}(\nu, \nu'n)^{180}\text{Ta}$ reactions in the ν process in stellar explosions. Another proposed site is the p process in O/Ne-rich layers in type-II supernovae (SNII), where the (γ, n) reactions on ^{181}Ta lead to ^{180}Ta production [5–8]. Finally, in low-mass asymptotic giant branch (AGB) stars, two reaction sequences have been suggested as sources for ^{180}Ta : (i) neutron capture on ^{179}Hf resulting in an isomeric state of ^{180}Hf ($J^\pi = 8^-, 1141$ keV), which has a small β decay branch to $^{180\text{m}}\text{Ta}$ and (ii) β decay of thermally excited states in ^{179}Hf to ^{179}Ta , and subsequent

neutron capture to $^{180\text{m}}\text{Ta}$ [9]. Figure 1 shows the two reaction paths with red and green arrows, respectively. Käppeler *et al.* [10] estimate that (ii) can explain 80%–86% of the solar ^{180}Ta abundance, while path (i) seems to only contribute to a small extent [11]. However, a recent study [8] modeled s -process nucleosynthesis in AGB stars using the neutron capture cross sections derived from statistical models (using experimentally obtained nuclear structure parameters [12]), and found only a negligible contribution to the observed ^{180}Ta abundance. They also studied the impact of the newly constrained value of the $^{179}\text{Ta}(n, \gamma)$ cross sections on the time-reversed reaction $^{180}\text{Ta}(\gamma, n)^{179}\text{Ta}$, which is the main mode of destruction of $^{180\text{m}}\text{Ta}$ in the SNII p process. They found that the new reaction rate reduces the $^{180\text{m}}\text{Ta}$ overabundance in the p -process models. The variety of different predictions emphasizes the need for accurate experimental data on nuclear reactions and stellar half-lives for the isotopes involved.

The destruction reaction $^{180\text{m}}\text{Ta}(n, \gamma)$ has been measured by Wisshak *et al.* [14]. A direct measurement of $^{179}\text{Ta}(n, \gamma)$ cross section at neutron energies relevant to s -process temperatures (keV neutron energies) has not been possible yet due to the lack of availability of a radioactive ^{179}Ta ($T_{1/2} = 1.82$ y) target with sufficient mass. However, the larger neutron fluxes available at research reactors allow an activation measurement of the $^{179}\text{Ta}(n, \gamma)^{180}\text{Ta}$ reaction at thermal-neutron energies (25 meV). There is only one previous measurement of the thermal $^{179}\text{Ta}(n, \gamma)^{180}\text{Ta}$ cross section and resonance integral [15]. This article reports the results of a new measurement of this important reaction cross section.

*Corresponding author: ruchi.garg.phys@gmail.com

†Deceased.

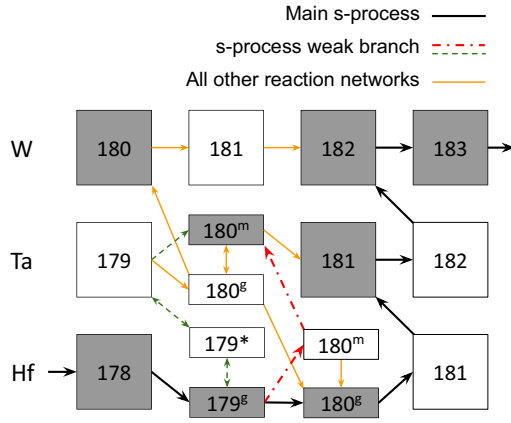


FIG. 1. *s*-process reaction network. Gray and white boxes show the stable and unstable isotopes respectively. Thick black arrows show the main *s*-process path. The red and green arrows show the weak branching paths suggested by Refs. [13] and [9], respectively. The orange arrows show all the other reactions in the network.

II. METHOD

A. Radioactive target production

The ^{179}Ta sample was produced via $^{180}\text{Hf}(p, 2n)$ reactions on a metallic Hf foil, using the same approach as Ref. [15]. The hafnium foil (>99.63% purity) of 1.331 g was irradiated for ≈ 7 hours with a 27-MeV beam of protons and a current of $32 \mu\text{A}$ at the MC40 cyclotron at the University of Birmingham. In addition to the isotope of interest, ^{179}Ta , the proton irradiation also produced a few other radioactive isotopes in the sample, the most dominant ones being $^{172, 175, 181}\text{Hf}$ and ^{172}Lu . After a cool-down period of ≈ 7 months, the sample was treated at PSI for the radio-chemical separation of ^{179}Ta as follows: The obtained Hf foil was partially dissolved in concentrated hydrofluoric acid (HF) with a few drops of HNO_3 . An aliquot of the sample was measured by a high-purity germanium (HPGe) detector to identify the main radioactive isotopes in the sample. The most dominant γ lines were attributed to ^{175}Hf and ^{172}Hf , together with its radioactive daughter ^{172}Lu . The hafnium isotopes were then conveniently used as tracers to follow the efficiency of the chemical separation of ^{179}Ta . After the dissolution, the sample was diluted by Milli-Q water, changing the HF concentration to 1 mol L^{-1} . The solution was then applied on a chromatographic column filled with TBP resin (Triskem). The majority of the hafnium in the solution passed through the column whereas ^{179}Ta was absorbed on the resin. Afterwards, ^{179}Ta was eluted using 0.1 M HCl solution. The decontamination factor, D , from hafnium was determined using

$$D = \frac{C_{\text{Hf}}^0}{C_{\text{Hf}}^s} \approx \frac{A_{^{175}\text{Hf}}^0}{A_{^{175}\text{Hf}}^s}, \quad (1)$$

where C^0 and C^s represent relative hafnium concentrations before and after the separation respectively, while A^0 and A^s represent the radioactivity of ^{175}Hf demonstrated by its 343.4 keV γ -ray emission from the sample before and after the

separation, respectively. The decontamination factor D was measured to be of the order of 300.

The solution containing ^{179}Ta was afterwards evaporated to near dryness and redissolved in a mixture of $6 \text{ mol L}^{-1} \text{ HCl}/20 \text{ mmol L}^{-1} \text{ HF}$. The solution was then applied to a chromatographic column containing 2 g of TEVA resin as described by Snow *et al.* [16]. The ^{179}Ta was absorbed in the column whereas hafnium was eluted as the column was washed with a fresh acid mixture. After no signal from ^{175}Hf could be detected with a HPGe detector, the ^{179}Ta was eluted from the column using $6 \text{ mol L}^{-1} \text{ HNO}_3/20 \text{ mmol L}^{-1} \text{ HF}$ mixture. After the γ spectroscopic analysis only a weak signal of ^{175}Hf was found in the eluate containing ^{179}Ta , yielding a minimum separation factor on the order of 1×10^4 . The separation procedure on TEVA resin was repeated once more without use of additional radiotracers in order to remove the last traces of hafnium from the sample. The extracted sample was sealed in the tip of an Eppendorf vial for transportation to Mainz for activation at the TRIGA reactor.

The activity of the extracted sample, as measured at Mainz on day 521 from the proton irradiation of the hafnium foil, was found to be 1.905(55) MBq. This activity corresponds to a ^{179}Ta mass of 47 ng or 1.58×10^{14} atoms. The activity was determined by measuring ^{179}Ta x-rays [17] at energies 54.61 and 55.79 keV of intensities 12.6(3)% and 21.8(5)%, respectively, on two identical low-energy HPGe detectors. The uncertainty on the measured activity was calculated by combining the uncertainties of the x-ray intensities, detection efficiencies, and the statistical error on the peak counts.

B. Reactor activation and Cd difference method

The $^{179}\text{Ta}(n, \gamma)^{180}\text{Ta}$ cross section was measured via the activation technique, which consists of exposing the sample to a flux of neutrons and subsequent counting of the reaction product ^{180}Ta through its radioactive decay. This allows the neutron capture cross section to be determined using

$$\sigma \Phi = \frac{N_{^{180}\text{Ta}}}{N_{^{179}\text{Ta}}}, \quad (2)$$

where $N_{^{179}\text{Ta}}$ and $N_{^{180}\text{Ta}}$ is the number of ^{179}Ta and ^{180}Ta nuclei, respectively. The neutron fluence (time integrated flux) Φ was determined by irradiation of isotopes with well-known cross sections (Table II) and $N_{^{180}\text{Ta}}$ was determined by decay counting of its 93.3 keV gamma line. It should be emphasized here that since the activation technique can only be used for reactions with a radioactive product, the present work only determines the cross section to the unstable ground state of ^{180}Ta .

Irradiation of the ^{179}Ta sample was performed at the TRIGA reactor in Mainz, in a rotating irradiation carousel, which results in exposure to a uniform neutron flux. The reactor's neutron energy spectrum is comprised of three main components: moderated thermal neutrons with a Maxwell-Boltzmann distribution corresponding to $kT = 25.3 \text{ meV}$, epithermal neutrons (0.2 eV–0.5 MeV) with the flux exhibiting a $1/E$ energy dependence, and fast fission neutrons ($E_n > 0.5 \text{ MeV}$). For the present experiment, the contribution from

TABLE I. Masses of the fluence monitor samples.

Activation	Sample	Mass (mg)
First: no shield	Au-1	$(5.91 \pm 0.01) \times 10^{-3}$
	Au-2	$(6.33 \pm 0.01) \times 10^{-3}$
	Zr-1	23.4 ± 0.1
	Zr-2	23.5 ± 0.1
Second: Cd shield	Au-3	$(5.91 \pm 0.01) \times 10^{-3}$
	Au-4	$(6.33 \pm 0.01) \times 10^{-3}$
	Zr-3	23.4 ± 0.1
	Zr-4	23.5 ± 0.1
	Sc-3	1.45 ± 0.01
	Sc-4	1.54 ± 0.01

fast neutrons to the cross section is negligible due to the low flux and low reaction cross sections.

In the presence of these different components of the neutron flux, the activation equation becomes

$$\sigma_{\text{th}}^{AX} \Phi_{\text{th}} + I_{\text{res}}^{AX} \Phi_{\text{epi}} = \frac{N_{A+1X}}{N_{AX}}, \quad (3)$$

where Φ_{th} and Φ_{epi} are the thermal and epithermal components of the neutron fluence, σ_{th}^{AX} is the cross section for a thermal-neutron capture on the AX nucleus, I_{res}^{AX} is the resonance integral of the cross section in the epithermal energy region, and N_{AX} and N_{A+1X} are the number of target nuclei and the activated nuclei, respectively.

To measure the contribution to the activation of the sample from the thermal and epithermal components of the fluence, the cadmium difference method was employed. This involved two irradiations of the ^{179}Ta sample, one with and one without a surrounding cadmium shield of 1 mm thickness, which shields the sample from thermal neutrons due to the high thermal absorption cross section of ^{113}Cd . Each irradiation was performed for 3 hours, 20 days apart to ensure that no ^{180}Ta was left in the sample before the second irradiation.

The neutron fluence (Φ_{th} and Φ_{epi}) that the ^{179}Ta sample was exposed to during the activations was measured using a combination of isotopes with well-known neutron-capture cross sections at thermal and epithermal energies. Two samples of each monitor isotope were placed on opposite sides of the ^{179}Ta sample during activations, allowing for the determination of the fluence at the ^{179}Ta location by averaging. The fluence monitor samples that were used in the two activations

TABLE II. List of isotopes used to measure neutron fluence. The cross-section values are taken from the Atlas of Neutron Resonances [18].

Isotope	Abundance(%)	σ_{thermal} (b)	I_{res} (b)
^{45}Sc	100	27.16 ± 0.20	12.0 ± 0.05
^{94}Zr	17.4 ± 0.3	0.0498 ± 0.0017	0.265 ± 0.01
^{96}Zr	2.8 ± 0.1	0.0229 ± 0.0010	5.15 ± 0.11
^{197}Au	100	98.67 ± 0.09	1550.0 ± 28.0

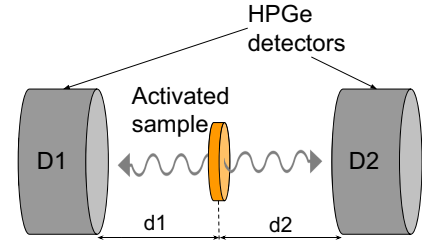


FIG. 2. Schematic diagram of the detector setup comprising of two identical HPGe detectors D1 and D2 placed at distances d_1 and d_2 from the source holder, respectively.

are listed in Table I. Table II lists the monitor isotopes along with their abundances and the (n, γ) cross sections at thermal and epithermal neutron energies. This combination of isotopes was chosen since the cross sections are already known with high accuracy and their excitation functions show different behavior.

C. Gamma-activity measurement

The gamma-activity of the irradiated samples (^{179}Ta and the fluence monitors) was measured using two identical HPGe detectors arranged as shown in Fig. 2. The sample was secured in a holder and the two detectors were placed at opposite sides of the sample. The whole setup was placed inside lead shielding to reduce background from natural radioactivity. The detectors were placed at 5 cm from the source holder to measure the activity from irradiated ^{179}Ta sample.

Tantalum-180 activity was measured using γ rays following the β decay of ^{180}Ta to the first 2^+ state of ^{180}Hf at 93.3 keV (with 4.51% intensity). At this low energy, the background from 55–65 keV x rays from ^{179}Ta was significant. Therefore, an indium absorber disk of 1.5 mm was placed in front of each detector for ^{180}Ta activity measurements. Figure 3 shows a γ -ray spectrum of the irradiated ^{179}Ta sample with the 93.3 keV line clearly marked.

The fluence monitor samples had a higher activity compared with the ^{179}Ta sample due to their higher mass. Therefore, their activity measurements required the detectors to be placed farther at ≈ 11 cm from the sample in order to reduce the dead time.

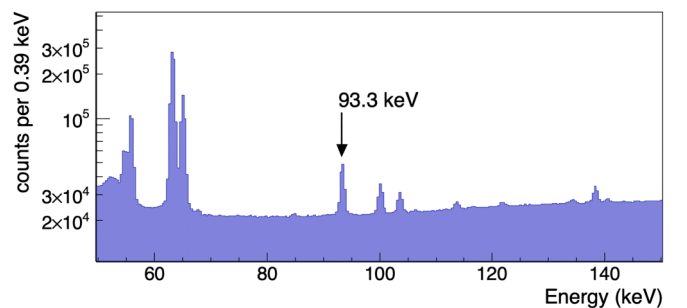


FIG. 3. Gamma-ray spectrum of activated ^{179}Ta as recorded in detector D1 (see Fig. 2) over 12 h starting 5.5 h after the irradiation.

III. DATA ANALYSIS AND RESULTS

A. Activation ratio

The activation ratio R is the number of activated nuclei divided by the number of target nuclei. This ratio for an irradiated sample was obtained using the following equation:

$$R = \frac{C_\gamma}{\epsilon(E_\gamma, d) I_\gamma f_a f_w f_m N_{\text{target}}}, \quad (4)$$

where

C_γ = counts in the characteristic γ peak,

$\epsilon(E_\gamma, d)$ = absolute detection efficiency at γ energy, E_γ ,

and detector distance d ,

I_γ = decay intensity of the characteristic γ line,

f_a = correction for decay during activation time, t_a

$$= \frac{1 - e^{-\lambda t_a}}{\lambda t_a},$$

f_w = correction for decay during waiting period, t_w

$$= e^{-\lambda t_w},$$

f_m = correction for decay during measurement time, t_m

$$= 1 - e^{-\lambda t_m},$$

λ = decay constant.

B. Efficiency of the detectors

To calculate the activation ratio of a sample using Eq. (4), the absolute detection efficiencies of the detectors were required at the sample's characteristic γ -ray energies and for the corresponding detection setup arrangement. GEANT3 simulations [19] of the setup accurately modeled the detector response as a function of γ -ray energy, the attenuation from an absorber of given thickness, and the geometrical acceptance of the setup for a given distance between detector and the source. Therefore, to obtain the absolute detection efficiencies, $\epsilon(E_\gamma, d)$, the only unknowns in the simulations were the distances of the detectors to the source-holder (d_1 and d_2 in Fig. 2).

To precisely determine the detector-to-sample-holder distances, the simulated efficiencies $\epsilon(E_\gamma, d)$ at different E_γ and d values (varying in the intervals of 1 mm) were compared with the efficiency values of the setup measured using the radioactive sources of well-known activities. The γ rays from the standard sources that were used, ^{241}Am , ^{133}Ba , ^{137}Cs , ^{109}Cd , and $^{57,60}\text{Co}$, covered the energy range corresponding to the characteristic γ -ray lines of fluence monitor isotopes (411 to 1120 keV) and the ^{180}Ta decay (93.3 keV). Table V lists the characteristic γ -ray lines for every isotope that was irradiated in the present work.

For the higher energy range (>200 keV) corresponding to the γ lines from the monitor isotopes, the detection efficiency can be described by the function,

$$\epsilon(E_\gamma) = A \exp[B + C \ln(E_\gamma) + D[\ln(E_\gamma)]^2], \quad (5)$$

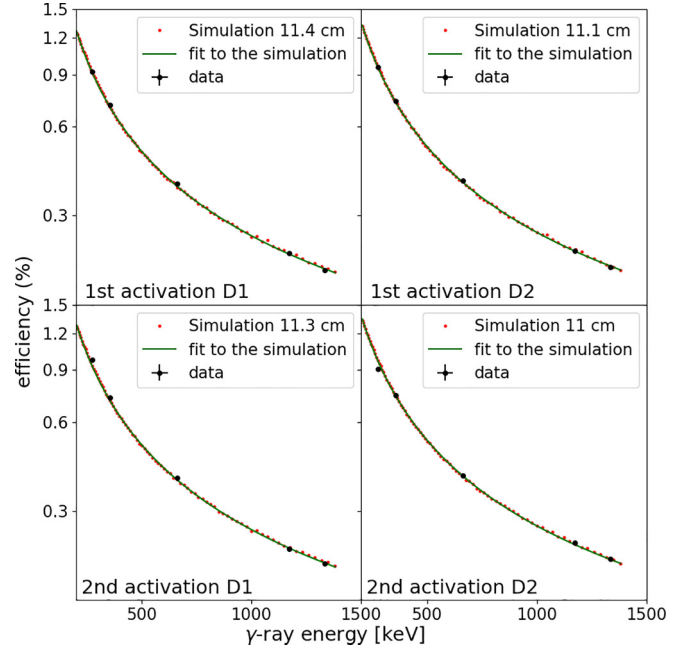


FIG. 4. Detector efficiency as a function of energy for the two detectors D1 and D2 for the fluence monitors' spectroscopy setups after the first (no shield) and second (Cd shield) activations. Black circles show the measured values using radioactive sources. Error bars on the measurements are smaller than then marker size. Red dots are the simulated values obtained using GEANT3. The green line is the fit to the simulated values.

where, A , B , C , and D are the free parameters. This function was used to fit the simulated $\epsilon(E_\gamma)$ values for the monitors' spectroscopy setup to obtain a continuous relationship between the energy and efficiency and evaluate the simulated efficiencies at the sources' γ energies. Finally, the detector distances were determined by minimizing the reduced- $\chi^2(d)$, given by the following equation:

$$\chi^2(d) = \sum_i \frac{[\epsilon^{\text{sim}}(E_i, d) - \epsilon^{\text{meas}}(E_i)]^2}{[\Delta \epsilon^{\text{meas}}(E_i)]^2}, \quad (6)$$

where ϵ^{sim} and ϵ^{meas} are the simulated and measured efficiencies, respectively, $\Delta \epsilon^{\text{meas}}$ is the uncertainty on the measured values, d is the detector-to-source-holder distance in the simulation, and E_i are the sources' γ -ray energies. The simulated distance that resulted in the least χ^2 was chosen as the best description of the real setup and was used to evaluate the detection efficiencies at the monitors' γ energies. Figure 4 shows the measured and best-match simulated efficiencies for the setup arrangements for fluence monitors' spectroscopy. The uncertainty in the detector distances was estimated to be 0.1 cm from the χ^2 variation as a function of distance. This translated to a relative uncertainty of $<1\%$ on the evaluated efficiencies.

A similar procedure was applied to evaluate the detector distances and thus the efficiencies for the tantalum sample's spectroscopy setup. In this case, however, the fit function from Eq. (5) could not be used because it is not valid in the low-

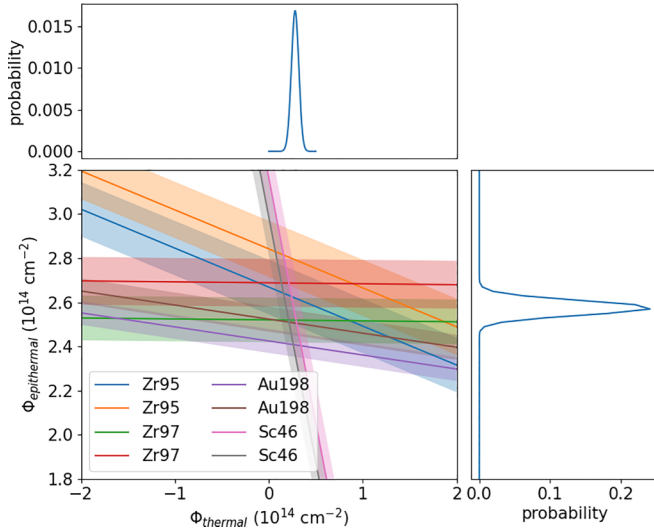


FIG. 5. Epithermal vs thermal fluence plots as measured with different monitor isotopes (two samples of each) in the second activation (with Cd shield). The top and the right plots give the probability distribution of the Φ_{th} and Φ_{epi} solutions, respectively.

energy region. Instead, the detector distances were determined by direct comparison of the measured efficiencies with the simulation of the detector response at the energies corresponding to the radioactive sources used. The simulations of this setup also accounted for the attenuation from the absorber disk that was placed in front of the detectors to reduce the x-ray background (Sec. II C). At 93.3 keV, corresponding to the ^{180}Ta γ -ray energy, we obtained efficiency values for detector1 (detector2) for the first and second activations of 6.18×10^{-3} (6.52×10^{-3}) and 6.40×10^{-3} (6.54×10^{-3}), respectively. The relative uncertainty on these efficiency values were 2.3%.

More details of the effect of the absorber thickness and the distance between sample and detectors on γ spectra can be found in Ref. [20].

C. Neutron fluence

For the first activation (without Cd shield), three monitor isotopes, i.e., ^{94}Zr , ^{96}Zr , and ^{197}Au , were sufficient to determine the fluence. The second activation (with Cd shield) required an additional monitor isotope with a higher sensitivity to the thermal neutrons due to the small thermal fluence. Scandium-45 has a high σ_{th} -to- I_{res} ratio, and therefore, was used as a monitor in the second activation.

For each activation, a set of linear equations for Φ_{th} and Φ_{epi} was obtained by inserting the activation ratios of the monitor isotopes [calculated using Eq. (4)] and the cross-section values (from Table II) in Eq. (3). Figure 5 shows the eight linear equations for the four monitor isotopes (two samples each) that were used in the second activation (without Cd shield). Since with several monitor reactions the equations are overdetermined, the fluence values Φ_{th} and Φ_{epi} were obtained by combining the $2d$ probability distributions for each monitor and normalizing the integral to one. The details of the technique can be found in Ref. [21].

TABLE III. Fluence and tantalum activation values for the irradiations with and without Cd shielding as measured using the two detectors. The average values of the fluences were calculated using the averaged activation values of the monitor isotopes in the procedure described in Sec. III C.

	Activation	Φ_{th} (10^{14} cm^{-2})	Φ_{epi} (10^{14} cm^{-2})	N_{180}/N_{179} (10^{-7})
Det. 1	No Cd	56.77 ± 1.39	2.62 ± 0.08	59.77 ± 3.06
	Cd	0.28 ± 0.04	2.60 ± 0.03	5.22 ± 0.39
Det. 2	No Cd	56.25 ± 1.40	2.64 ± 0.08	58.52 ± 2.68
	Cd	0.28 ± 0.04	2.56 ± 0.03	5.70 ± 0.41
Avg.	No Cd	56.49 ± 1.31	2.63 ± 0.08	59.15 ± 2.75
	Cd	0.28 ± 0.04	2.58 ± 0.03	5.46 ± 0.33

The fluence values for both activations from each of the detector measurements are listed in Table III. The excellent agreement between the values obtained from the two detectors is notable as each detector was treated independently in terms of dead time, efficiencies, and γ -peak integration.

D. Cross-section calculations

The measured activation ratios ($N_{180\text{Ta}}/N_{179\text{Ta}}$) for the two activations of ^{179}Ta sample are given in last column of the Table III. The activation values were calculated using Eq. (4).

Using the fluence and activation ratio values from the two activations (Table III) in Eq. (3), the following set of two linear equations was obtained, that was solved for thermal cross-section σ_{th} and the resonance integral I_{res} of ^{179}Ta :

$$\sigma_{th} \Phi_{th} + I_{res} \Phi_{epi} = \frac{N_{180\text{Ta}}}{N_{179\text{Ta}}}, \quad (7a)$$

$$\sigma_{th} \Phi_{th}^{Cd} + I_{res} \Phi_{epi}^{Cd} = \frac{N_{180\text{Ta}}}{N_{179\text{Ta}}}\bigg|_{Cd}. \quad (7b)$$

The final cross-section results are shown in Table IV.

The uncertainties on the final cross-section values were calculated from the standard error propagation of the uncertainties on fluence and tantalum activation values that are listed in Table III. The uncertainties on the fluence values (Table III) were determined as the standard deviation in the probability distribution that were obtained in Sec. III as shown in Fig. 5, which in turn were dependent on the uncertainties in the cross sections of the monitors isotopes and their activation ratios. Given that the parameters in the activation ratio (4) were uncorrelated, their uncertainties were combined in the

TABLE IV. $^{179}\text{Ta}(n, \gamma) ^{180}\text{Ta}^{g.s.}$ reaction cross section as measured in the present work. The average column values were calculated using the average fluence and activation values from Table III.

	σ_{th} (b)	I_{res} (b)
Detector 1	965 ± 63	1905 ± 167
Detector 2	939 ± 57	2125 ± 180
Average	952 ± 57	2013 ± 148

TABLE V. Relative uncertainties in percentage on variables in the activation Eq. (4). The uncertainties on peak counts, efficiencies, and activation ratio for both detectors were similar. The values shown here are for detector D1. The uncertainties for the fluence monitors listed here are for a typical sample per isotope (out of all that are listed in Table I).

Sample	Au-4	Zr-4		Sc-4	Ta(No-Cd/Cd)	
	¹⁹⁸ Au	⁹⁵ Zr	⁹⁷ Zr	⁴⁶ Sc	¹⁸⁰ Ta	
E_γ (keV)	411.8	724.2, 756.7	743.4	1120.5	93.3	
$\Delta C_\gamma/C_\gamma$	0.68	3.22, 2.22	0.28	0.64	1.22	5.44
$\Delta \epsilon_\gamma/\epsilon_\gamma$	1.00	1.00, 1.00	1.00	1.00	2.29	2.29
$\Delta I_\gamma/I_\gamma$	0.10	0.50, 0.40	0.17	0.00	3.55	
$\Delta f_a/f_a$	0.56	0.56	0.56	0.56	0.58	0.58
$\Delta f_w/f_w$	0.00	0.00	0.19	0.00	0.30	0.30
$\Delta f_m/f_m$	0.00	0.00	0.03	0.00	0.02	0.04
$\Delta N_{tar}/N_{tar}$	0.17	0.14	0.14	0.65	2.55	2.58
$\Delta R/R$	1.35	2.74	3.44	1.46	5.12	7.38

standard way to obtain the uncertainties on the activation ratios. Table V lists the relative uncertainties on the variables of Eq. (4) for the tantalum sample and the fluence monitor samples numbered four (selected randomly).

IV. SUMMARY AND DISCUSSION

In present work, we have measured the neutron-capture cross section on ¹⁷⁹Ta at thermal and epithermal neutron energies via activation technique at TRIGA reactor, Mainz. The high neutron fluence at the reactor allowed for a cross-section measurement using only a 47 ng sample of ¹⁷⁹Ta. The target was produced via the ¹⁸⁰Hf(*p*, 2*n*)¹⁷⁹Ta reactions at MC40 cyclotron at the University of Birmingham, and the irradiated material was processed at PSI into a target.

We obtain a thermal cross-section value of 952 ± 57 b, and a resonance integral of $I_{res} = 2013 \pm 148$ b (see Table IV). The only previous experimental data on the ¹⁷⁹Ta(*n*, γ) reaction are by Schumann and Käppeler [15], who obtained 932 ± 62 and 1216 ± 69 b for σ_{th} and I_{res} , respectively. While the agreement for the thermal values is excellent, our resonance integral is 1.66 times higher. The reason for this large discrepancy is unknown. In both measurements, the same thickness (1 mm) of the Cd absorber was used. Any small inhomogeneities in the thickness would not lead to significantly

different results in the two measurements, unless there is a strong resonance in the ¹⁷⁹Ta + *n* reaction at neutron energies around the cut off (0.1–1 eV) [22]. However, at present, there is no experimental data on neutron resonances for this reaction. We therefore strongly encourage the investigation of the ¹⁷⁹Ta + *n* reaction in the eV-energy-regime at a time-of-flight facility.

The higher-resonance integral may point to a higher neutron capture cross section in the stellar neutron energy (keV) range, which would lead to a higher production of ¹⁸⁰Ta during the *s* process. For any firm conclusions, however, a measurement of the cross section at stellar energies is required. In addition, cross-section data on production of the isomeric state ^{180m}Ta are essential. This can be achieved by combining an activation measurement with a neutron time-of-flight study, the latter allowing determination of the total production of ¹⁸⁰Ta, i.e., ¹⁸⁰Ta^{*m*} + ¹⁸⁰Ta^{*g.s.*}.

ACKNOWLEDGMENTS

This work was supported by the UK Science and Facilities Council (ST/M006085/1, ST/V001043/1), European Research Council ERC-2015-StG Nr. 677497, and the HORIZON 2020 SANDA Project No. 847552.

- [1] S. E. Woosley, D. H. Hartmann, R. D. Hoffman, and W. C. Haxton, *Astrophys. J.* **356**, 272 (1990).
- [2] A. Heger, E. Kolbe, W. C. Haxton, K. Langanke, G. Martínez-Pinedo, and S. E. Woosley, *Phys. Lett. B* **606**, 258 (2005).
- [3] T. Hayakawa, T. Kajino, S. Chiba, and G. J. Mathews, *Phys. Rev. C* **81**, 052801(R) (2010).
- [4] A. Sieverding, G. Martínez-Pinedo, L. Huther, K. Langanke, and A. Heger, *Astrophys. J. Lett.* **865**, 143 (2018).
- [5] N. Prantzos, M. Hashimoto, M. Rayet, and M. Arnould, *Astron. Astrophys.* **238**, 455 (1990).
- [6] M. Rayet, M. Arnould, M. Hashimoto, N. Prantzos, and K. Nomoto, *Astron. Astrophys.* **298**, 517 (1995).
- [7] H. Utsunomiya, H. Akimune, S. Goko, M. Ohta, H. Ueda, T. Yamagata, K. Yamasaki, H. Ohgaki, H. Toyokawa, Y.-W. Lui, T. Hayakawa, T. Shizuma, E. Khan, and S. Goriely, *Phys. Rev. C* **67**, 015807 (2003).
- [8] K. L. Malatji, M. Wiedeking, S. Goriely, C. P. Brits, B. V. Kheswa, F. L. Bello Garrote, D. L. Bleuel, F. Giacoppo, A. Görgen, M. Guttormsen, K. Hadynska-Klek, T. W. Hagen, V. W. Ingeberg, M. Klintejord, A. C. Larsen, P. Papka, T. Renstrøm, E. Sahin, S. Siem, L. Siess *et al.*, *Phys. Lett. B* **791**, 403 (2019).
- [9] K. Yokoi and K. Takahashi, *Nature (London)* **305**, 198 (1983).
- [10] F. Käppeler, C. Arlandini, M. Heil, F. Voss, K. Wisshak, R. Reifarh, O. Straniero, R. Gallino, S. Masera, and C. Travaglio, *Phys. Rev. C* **69**, 055802 (2004).
- [11] S. E. Kellogg and E. B. Norman, *Phys. Rev. C* **46**, 1115 (1992).
- [12] C. P. Brits, K. L. Malatji, M. Wiedeking, B. V. Kheswa, S. Goriely, F. L. Bello Garrote, D. L. Bleuel, F. Giacoppo, A. Görgen, M. Guttormsen, K. Hadynska-Klek, T. W. Hagen,

- S. Hilaire, V. W. Ingeberg, H. Jia, M. Klintefjord, A. C. Larsen, S. N. T. Majola, P. Papka, S. Péru *et al.*, *Phys. Rev. C* **99**, 054330 (2019).
- [13] H. Beer and R. A. Ward, *Nature (London)* **291**, 308 (1981).
- [14] K. Wisshak, F. Voss, C. Arlandini, F. Bečvář, O. Straniero, R. Gallino, M. Heil, F. Käppeler, M. Krtička, S. Masera, R. Reifarth, and C. Travaglio, *Phys. Rev. Lett.* **87**, 251102 (2001).
- [15] M. Schumann and F. Käppeler, *Phys. Rev. C* **60**, 025802 (1999).
- [16] M. S. Snow, M. R. Finck, K. P. Carney, and S. S. Morrison, *J. Chromatogr. A* **1484**, 1 (2017).
- [17] C. M. Baglin, Nuclear data sheets for $A = 179$, *Nucl. Data Sheets* **110**, 265 (2009).
- [18] S. Mughabghab, *Atlas of Neutron Resonances*, 5th ed. (Elsevier Science, Amsterdam, 2006).
- [19] R. Brun, F. Bruyant, M. Maire, A. C. McPherson, and P. Zandarini, GEANT3 (1987).
- [20] S. Dellmann, Master's thesis, Goethe-Universität, 2021 (unpublished).
- [21] S. Dellmann, R. Reifarth, M. Weigand, K. Eberhardt, R. Garg, C. Geppert, T. Heftrich, D. Kurtulgil, and C. Lederer-Woods, *EPJ Web Conf.* **260**, 11035 (2022).
- [22] E.-I. Esch, R. Reifarth, E. M. Bond, T. A. Bredeweg, A. Couture, S. E. Glover, U. Greife, R. C. Haight, A. M. Hatarik, R. Hatarik, M. Jandel, T. Kawano, A. Mertz, J. M. O'Donnell, R. S. Rundberg, J. M. Schwantes, J. L. Ullmann, D. J. Vieira, J. B. Wilhelmy, and J. M. Wouters, Measurement of the $^{237}\text{Np}(n, \gamma)$ cross section from 20 meV to 500 keV with a high efficiency, highly segmented 4π BaF₂ detector, *Phys. Rev. C* **77**, 034309 (2008).